Materials International
Open Access Journal (ISSN: 2668-5728)

Article
Volume 6, Issue 4, 2024, 36
https://doi.org/10.33263/Materials64.036

Mixed Convection of Heat and Mass Transfer of Casson Fluid Flow Over a Moving Horizontal Plate with Convective Boundary Conditions

Veena B. Nagendra [1,*], Srikantha Narasimhamurthy [1], Sushma Shankar [1], Uma Munivenkatappa [1]

[1] Department of Mathematics, M. S. Ramaiah Institute of Technology, Bengaluru, India (Affiliated to VTU); mvymath@gmail.com (V.B.N.); srikantha087@gmail.com (S.N.); sush.msrit@gmail.com (S.S.); umashivaram@gmail.com (U.M.);
* Correspondence: mvymath@gmail.com;
Scopus Author ID 6507741440

Received: 13.03.2024; Accepted: 6.10.2024; Published: 10.12.2024

Abstract: This research article primarily explores mixed convection involving a Casson fluid as it flows over a horizontally moving plate. To tackle this, the study initiates by converting the partial differential equations (PDEs) that delineate fluid flow and the accompanying convective boundary conditions into ordinary differential equations (ODEs). This conversion is achieved by applying a dimensionless similarity transformation (ST) and utilizing the one-parameter continuous group method. Subsequently, the acquired ODEs are systematically solved using a combination of the finite difference method and a specialized 'dsolve' technique based on Richardson extrapolation. This innovative approach enhances the precision and efficiency of ODE solutions. The paper extensively investigates how several features, together with the properties of the Casson fluid and other applicable parameters, influence the flow variables. These discoveries are visually depicted through graphical representations, offering a lucid and insightful comprehension of the intricacies of this mixed convection scenario.

Keywords: Casson fluid; convective boundary conditions; mixed convection; horizontal plate; chemical reaction.

1. Introduction

Fluids are a unique type of matter that can flow and undergo distortion when external force is applied. Different fluids exist, such as ideal, real, Newtonian, non-Newtonian, and ideal plastic fluids. Various fluids found in both biotechnological and manufacturing frameworks, some of them are ceramics, paints, blood, liquid detergents, polymers, lubricating greases, gypsum pastes, multi-grade oils, printer inks, diverge from the typical viscosity which obeys Newton's law, such fluids are called non-Newtonian fluids. Owing to their exhaustive benefits in various fields, budding researchers are studying and investigating the attributes of non-Newtonian fluids.

Uma *et al*. [1] investigated solute transfer in their problem, considering that the stretching surface deviated exponentially. Al-Kouz and Owhaib [2] studied the 3-D flow considering Casson nanofluid stretched linearly, taking a flat surface with a rotating frame. In another study, Animasaun *et al*. [3] examined Casson fluid and the movement of an incompressible laminar flow over a surface by considering the surface stretched exponentially with free convective MHD. They considered the special effects of flexible dynamic viscosity, thermal conductivity, and exponentially decaying heat generation internally. The study was conducted using an approximate analytical homotopy analysis method.

Bilal *et al*. [4] used the integral transform technique to investigate the Casson fluid over inclined isothermal considering riga surface in the presence of chemically reactive species with radiation effect. In another study, Mahanthesh *et al*. [5] explored the movement of magneto-Casson nanofluid owed to the surface gradient subjected to the Cattaneo–Christov heat flux law taking disk surface. Fan *et al*. [6] numerically analyzed heat and mass transfer of continuous moving plates by adopting transformation group theory by taking horizontal surfaces with mixed convective. They solved the similarity equations obtained using the 4^{th}-order Runge-Kutta method. Khashi'ie *et al*. [7] studied heat transfer on a moving plate in the presence of MHD hybrid nanoparticles with Joule heating by considering Cu-Al_2O_3/H_2O and horizontal geometry. They obtained two solutions when the plate moved opposite the free stream flow. Rohni *et al*. [8] conducted a theoretical investigation for the steady 2-D boundary–layer flow past a moving plate in the presence of different nanoparticles in water. Pramanik [9] investigated the boundary layer flow of the Casson fluid with the combined effect of suction and blowing over a sheet stretched exponentially. Khan *et al*. [10] considered mixed convection with variable concentration reactant and variable concentration along with chemical reaction with higher order in the flow of the Newtonian fluid. Sushma *et al*. [11] conducted a numerical analysis of the impact of fluctuating thickness, chemical reaction, and magnetic field on a sheet stretched in the context of Casson fluid. Shaw *et al*. [12] investigated Casson fluid flow in permeable convective boundary conditions taking horizontal plates. Sulochana and Poornima [13] examined the change of unsteady Casson fluid flow subjected to Lorentz force along a vertical plate, considering the presence of Hall current. They analytically solved the transformed nonlinear ODEs using the perturbation technique. Khan *et al*. [14] reviewed the effect of heat emission and thermal generation in the Casson fluid flow through a permeable medium and over the stretching sheet, employing the homotopy analysis method.

Pulsatile flows are encountered in diverse engineering, physiological, and industrial contexts. To connect these applications to real-world scenarios, Thamaraikannan *et al*. [15] and Kumar *et al*. [16] investigated the dynamics of unsteady pulsating flow involving Casson nanofluid through a porous channel, employing the perturbation technique. Srinivas *et al*. [17] investigated the effects of thermal radiation and chemical reaction in the heat and mass transfer of the pulsating flow of Casson fluid in a porous channel in the presence of an applied magnetic field. Sushma *et al*. [18] looked into the effects of triple diffusion on MHD Casson fluid flow through a vertical wall using numerical methods and convective boundary conditions.

Alwawi *et al*. [19] investigated the heat transfer characteristics of a Casson nanofluid in carboxymethyl, cellulose-water solution (CMC-water) around a solid sphere under mixed convection with the influence of a variable-strength magnetic field. Several numerical studies on Casson fluid in the presence of nanoparticles and multi-walled carbon nanotubes have been conducted previously [20-22]. The results obtained indicate that the presence of nanoparticles enhances heat transfer.

According to El-Zahar *et al*. [23], non-Newtonian nanofluids have improved thermal properties due to the presence of nanoparticles. Due to its diverse applications across various disciplines, the researchers employed theoretical analysis to investigate the magneto-flow characteristics of Casson hybrid nanofluid on a continuously moving/fixed surface under substantial suction.

A numerical investigation was conducted by Atashafrooz [24] to examine the impact of buoyancy forces on mixed convection heat transfer when nanofluids are present. The investigation utilized the finite volume method. The study also analyzed entropy generation effects within an inclined duct. Lone *et al.* [25] work investigates incompressible magnetohydrodynamic flow in the laminar, steady, for a non-Newtonian Casson fluid past a stratified extending sheet, incorporating various factors such as thermophoresis, heat source, bio-convection, Brownian motion, thermal radiation, and chemically reactive activation energy. Priyanka *et al.* [26] have observed that the Forchheimer parameter has a repellent effect on liquid motion, leading to a decrease in velocity magnitude within the boundary layer. Simultaneously, in the thermal boundary layer, there is an augmentation in the thermal profile. Vishalakshi *et al.* [27] offer a solution to stretching sheet issues by utilizing the Appell hypergeometric form. Additionally, the investigation delves into the impact of a time relaxation parameter.

In response to the rising demand for non-Newtonian nanofluid applications in industry and engineering, the research papers [28-30] focus on the flow of Casson nanofluid over a nonlinear stretching surface with accompanying effects. The advantages of the Casson nanofluid become evident, particularly in cooling and friction reduction applications, surpassing the performance of nanofluids based on Newtonian principles. The applications of nanofluids in heat and mass transfer are diverse and widespread, encompassing various fields of science and engineering. Researchers [31-35] have explored the behavior of nanofluids, particularly those involving Casson or Casson nanofluids, on stretching sheets. These studies contribute to understanding how these unique fluid systems impact heat and mass transfer processes, offering insights applicable to fields such as thermal management in electronics, renewable energy systems, and various industrial processes. The investigation of stretching sheets in the presence of Casson or Casson nanofluid provides valuable knowledge for optimizing heat transfer performance and enhancing the efficiency of these applications.

Many studies in the literature survey overlooked the consideration of the boundary conditions and effects over a horizontally moving plate. To fill this knowledge gap, exploring the laminar flow of an incompressible viscous Casson fluid under mixed convective boundary conditions over a horizontally moving plate influenced by non-uniform plate velocity is essential.

2. Materials and Methods

Nomenclature

$\boldsymbol{a, b, d, e}$	**Group parameter**
a^*	Velocity slip parameter
C	Concentration (Kg)
C_∞	Ambient concentration (Kg)
C_{fx}	Local Skin friction coefficient
C_w	Concentration at the lower plate (Kg)
D	Diffusion coefficient $(m^2\ s^{-1})$
$f(\eta)$	Non dimensional velocity
g	gravitational acceleration $(m^2\ s^{-2})$
Gr_T, Gr_C	Thermal and Solutal Grashof number
h_0	Constant
$h_f(x)$	Heat transfer coefficient (W/m^2K)
α	Thermal diffusivity $(m^2\ s^{-1})$
β	Casson parameter

$\boldsymbol{a, b, d, e}$	**Group parameter**
β_C	Volumetric concentration coefficient (Kg^{-1})
β_T	Volumetric thermal coefficient (K^{-1})
$(\Delta C)_0$	Constant
$(\Delta T)_0$	Constant
γ	Convective heat transfer parameter
k_0	Reaction rate constant
k	Thermal conductivity (W/mK)
K	Reaction rate parameter (Ms^{-1})
L	Length(m)
λ_1	Thermal buoyancy parameter
λ_2	Concentration buoyancy parameter
Nu_x	Local Nusselt number
n	Reaction order
ν	Kinematic viscosity $(m^2\ s^{-1})$
P	Pressure (Kg/ms^2)
$\Phi(\eta)$	Non dimensional concentration
q_w	Wall heat flux (Wm^{-2})
ρ	Density$(\ Kgm^{-3})$
ψ	Stream function
T	Temperature (K)
T_∞	Ambient temperature (K)
$T_f(x)$	Hot fluid temperature (K)
τ_w	Wall shear stress (Nm^{-2})
$\theta(\eta)$	Non dimensional temperature
u	Velocity component in x direction (ms^{-1})
U_0	Constant
$U(x)$	Non-uniform velocity (ms^{-1})
v_0	Constant (ms^{-1})
v	Velocity component y direction (ms^{-1})
$v_w(x)$	Velocity normal to plate (ms^{-1})
x, y	Cartesian coordinates (m)
ACRONYM	
ODE	Ordinary differential equation
PDE	Partial differential equations
ST	Similarity transformation

The present investigation depicts the laminar flow of an incompressible viscous fluid with mixed convective boundary conditions over a horizontal plate. The flow is triggered due to the horizontal motion of the plate with a non-uniform velocity U(x). The lower plate is heated through convection and is hot with the temperature $T_f(x)$ furnishing heat transfer coefficient $h_f(x)$ with concentration $C_w(x)$.

T_∞ , C_∞ represent the ambient temperature and ambient concentration of the fluid, respectively, as shown in Figure(1).

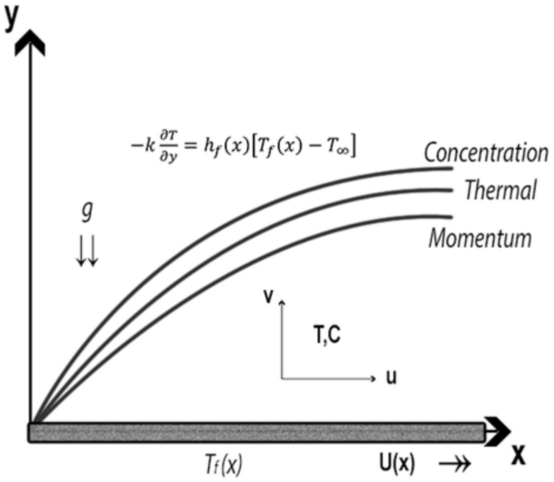

Figure 1. Flow geometry.

On the application of boundary layer approximation, the governing flow takes the form mentioned below. In the energy equation, the viscous dissipation term is neglected [19-23].

The governing equations are:

$$\frac{\partial u}{\partial x} + \frac{\partial v}{\partial y} = 0 \tag{1}$$

$$u\frac{\partial u}{\partial x} + v\frac{\partial u}{\partial y} = -\frac{1}{\rho}\frac{\partial P}{\partial x} + \nu\left(1 + \frac{1}{\beta}\right)\frac{\partial^2 u}{\partial y^2} \tag{2}$$

$$\frac{-1}{\rho}\frac{\partial P}{\partial y} + g(T - T_\infty)\beta_T + g(C - C_\infty)\beta_C = 0 \tag{3}$$

$$u\frac{\partial T}{\partial x} + v\frac{\partial T}{\partial y} = \alpha\frac{\partial^2 T}{\partial y^2} \tag{4}$$

$$u\frac{\partial C}{\partial x} + v\frac{\partial C}{\partial y} = D\frac{\partial^2 C}{\partial y^2} - k_0(C - C_\infty)^n \tag{5}$$

Boundary conditions:

At $y = 0$:

$$u = U(x),\ v = 0, -k\frac{\partial T}{\partial y} = h_f(x)\left[T_f(x) - T_\infty\right],\ C = C_w(x) \tag{6}$$

At $y \to \infty$:

$$u \to 0,\ \frac{\partial u}{\partial y} \to 0,\ T \to T_\infty,\ C \to C_\infty \tag{7}$$

Now introduce the stream function, dimensionless variables for temperature and concentration, ψ, θ, and Φ, respectively as:

$$u = \frac{\partial \psi}{\partial y}\ ,\ v = -\frac{\partial \psi}{\partial x},\ \theta = \frac{T - T_\infty}{T_f - T_\infty}, \quad \Phi = \frac{C - C_\infty}{C_w - C_\infty} \tag{8}$$

On substitution of Eq. (8) in Eqs. (1)- (5) by eliminating the pressure gradient, the set of equations so obtained are as follows:

$$\nu\left(1 + \frac{1}{\beta}\right)\frac{\partial^4 \psi}{\partial y^4} - \frac{\partial \psi}{\partial y}\frac{\partial^3 \psi}{\partial x \partial y^2} + \frac{\partial \psi}{\partial x}\frac{\partial^3 \psi}{\partial y^3} - g\beta_T\frac{\partial}{\partial x}(\theta\Delta T) - g\beta_T\frac{\partial}{\partial x}(\Phi\Delta C) = 0 \tag{9}$$

$$\alpha\frac{\partial^2}{\partial y^2}(\theta\Delta T) + \frac{\partial \psi}{\partial x}\frac{\partial}{\partial y}(\theta\Delta T) - \frac{\partial \psi}{\partial y}\frac{\partial}{\partial x}(\theta\Delta T) = 0 \tag{10}$$

$$D\frac{\partial^2}{\partial y^2}(\Phi\Delta C) + \frac{\partial \psi}{\partial x}\frac{\partial}{\partial y}(\Phi\Delta C) - \frac{\partial \psi}{\partial y}\frac{\partial}{\partial x}(\Phi\Delta C) - K_0(\Phi\Delta C)^n = 0 \tag{11}$$

On substituting Eq. (8), the boundary conditions in Eqs. (6) and (7) become:

At $y = 0$

$$\frac{\partial \psi}{\partial y} = U(x)\ ,\ \frac{\partial \psi}{\partial x} = 0,\ \frac{\partial \theta}{\partial y} = -\frac{h_f(x)}{k}[1 - \theta(0)],\ \Phi = 1 \tag{12}$$

At $y \to \infty$

$$\frac{\partial\psi}{\partial y} \to 0, \frac{\partial^2\psi}{\partial y^2} \to 0, \theta \to 0, \Phi \to 0 \quad (13)$$

2.1. Solution procedure.

Following the procedure followed by Fan *et al.* [6] and Khan *et al.* [10] to derive dimensionless transformations, we obtained the following transformations based on the applications of group theory. To convert Eqs. (9)-(11) to dimensionless form, we use the following dimensionless transformations:

$$\eta = \sqrt{Re}\frac{y}{L}\left(\frac{x}{L}\right)^a, \psi = \nu\sqrt{Re}\left(\frac{x}{L}\right)^b f(\eta), \theta = \theta(\eta), \Phi = \Phi(\eta), \Delta T = (\Delta T)_0\left(\frac{x}{L}\right)^d,$$

$$\Delta C = (\Delta C)_0\left(\frac{x}{L}\right)^d, U = U_0\left(\frac{x}{L}\right)^e, v_w = v_0\left(\frac{x}{L}\right)^a, h_f(x) = h_0\left(\frac{x}{L}\right)^a.$$

Here:

$$a = \frac{2n-2}{7-5n}, b = \frac{5-3n}{7-5n}, d =, e = \frac{3-n}{7-5n} \quad (14)$$

By plugging Eq. (14) in Eqs. (9)-(11) we get the following set of ODEs:

$$\left(1+\frac{1}{\beta}\right)f''''(\eta) + \left(\frac{5-3n}{7-5n}\right) f(\eta)f'''(\eta) - \left(\frac{n+1}{7-5n}\right)f'(\eta)f''(\eta) - \lambda_1\left[\left(\frac{2n-2}{7-5n}\right)\eta\theta'(\eta) + \left(\frac{4}{7-5n}\right)\theta(\eta)\right] - \lambda_2\left[\left(\frac{2n-2}{7-5n}\right)\eta\Phi'(\eta) + \left(\frac{4}{7-5n}\right)\Phi(\eta)\right] = 0 \quad (15)$$

$$\frac{1}{Pr}\theta''(\eta) + \left(\frac{5-3n}{7-5n}\right) f(\eta)\theta'(\eta) - \left(\frac{4}{7-5n}\right) f'(\eta)\theta(\eta) = 0 \quad (16)$$

$$\frac{1}{Sc}\Phi''^{(\eta)} + \left(\frac{5-3n}{7-5n}\right) f(\eta)\Phi'(\eta) - \left(\frac{4}{7-5n}\right) f'(\eta)\Phi(\eta) - K\Phi^n = 0 \quad (17)$$

Boundary conditions in Eq. (12) and (13) on using Eq. (14) become:

$$f(0) = 0, f'(0) = 1, \theta'(0) = -\gamma[1-\theta(0)], \Phi(0) = 1,$$

$$f'(\infty) = f''(\infty) = \theta(\infty) = \Phi(\infty) = 0 \quad (18)$$

Where:

$$Pr = \frac{\nu}{\alpha}, Sc = \frac{\nu}{D}, Re = \frac{U_0L}{\nu}, \gamma = \frac{Lh_0}{Re}, Gr_T = \frac{g\beta_{c(\Delta T)_0 L^3}}{\nu^2}, Gr_C = \frac{g\beta_{c(\Delta C)_0 L^3}}{\nu^2},$$

$$\lambda_1 = \frac{Gr_T}{Re^{2.5}}, \lambda_2 = \frac{Gr_C}{Re^{2.5}}, K = \frac{L^2k_0(\Delta C)_0^{n-1}}{\nu Re} \quad (19)$$

In the previous equations, $Pr \to$ Prandtl number, $Sc \to$ Schmidt number, $\lambda_1, \lambda_2 \to$ thermal and concentration buoyancy parameter, $Re \to$ Reynolds number, $\gamma \to$ Convective heat transfer parameter, $Gr_T, Gr_C \to$ thermal and solutal Grashof number, $K \to$ chemical reaction parameter.

Below are the definitions of the empirical quantities of interest in the present study: the local skin friction coefficient, the local Nusselt number, and the local Sherwood number.

2.2. Local Skin friction coefficient.

$$C_{fx} = -\frac{\tau_w}{\rho U^2}, \text{ where } \tau_w = \mu\left(\frac{\partial u}{\partial y}\right)_{y=0}$$

$$\left(\frac{x}{L}\right)^b C_{fx} = -\frac{f''(0)}{\sqrt{Re}} \quad (20)$$

2.3. Local Nusselt number.

$$Nu_x = \frac{-xq_w}{k\Delta T}, \text{ where } q_w = k\left(\frac{\partial T}{\partial y}\right)_{y=0}$$

$$\left(\frac{x}{L}\right)^{-(a+1)} Nu_x = -\sqrt{Re}\,\theta'(0) \quad (21)$$

2.4. Local Sherwood number.

$$Sh_x = \frac{-x m_w}{D \Delta C}, \text{ where } m_w = D\left(\frac{\partial C}{\partial y}\right)_{y=0}$$

$$\left(\frac{x}{L}\right)^{-(a+1)} Sh_x = -\sqrt{Re}\,\Phi'(0) \qquad (22)$$

3. Results and Discussion

Numerical solutions were obtained for the system of ODEs (15)-(17) with the application of STs (Eq. (14)), which were derived from a one-parameter continuous group method. The finite difference method and the Richardson extrapolation-based dsolve routine were used to solve the system. The effects of various parameters are discussed below. The parameters' range is carefully selected to ensure visibility of velocity, temperature, and concentration profile variations. Additionally, the physical significance of parameters is taken into account.

3.1. Effect on the velocity field.

Here, we discuss the effects of different parameters like the Chemical Reaction rate parameter, K; thermal buoyancy parameters, λ_1; concentration buoyancy parameters, λ_2; and Casson parameter, β ; on the velocity field by fixing the other parameters as constants.

Graphically, on examining Figure 2, it is observed that an overshooting of the velocity profile exists with respect to the moving horizontal plate.

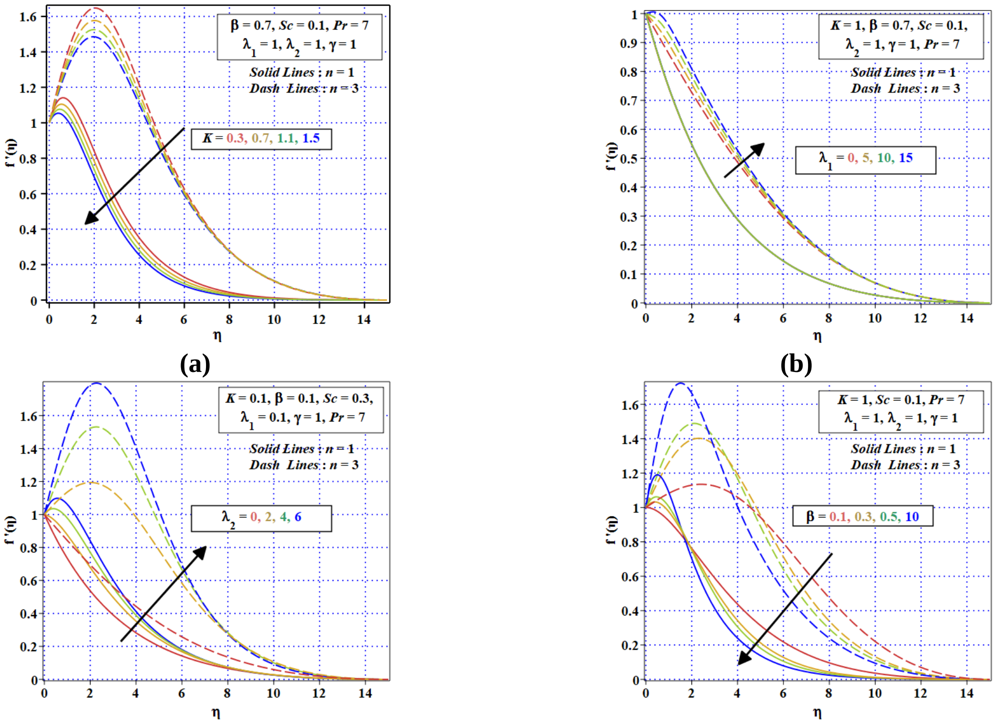

(c) (d)

Figure 2. (a,b) Graphs of velocity profiles for various K, λ_1 values; **(c,d)** graphs of velocity profiles for various λ_2, β values.

Figure 2(a) depicts the effects of the chemical reaction parameter for order $n = 1$ and $n = 3$ on the velocity profile. It is observed that when K increases, velocity boundary layer thickness decreases. From Figure 2(b) and 2(c) it is clear that as λ_1 and λ_2 increase the velocity profiles over the horizontal plate increases. In addition, there exists an overshooting for varying values of λ_2 near the boundary.

In Figure 2(d), initially, an increase in velocity profile near the boundary with the increase in β is observed later, and there exists a revert effect. This is because fluid becomes more viscous, which in turn reduces the fluid motion.

3.2. Effect on the temperature field.

Here, non-dimensional temperature $\theta(\eta)$ for different values of the key parameters λ_1, λ_2, Pr, β, Sc, γ are plotted in Figure 3.

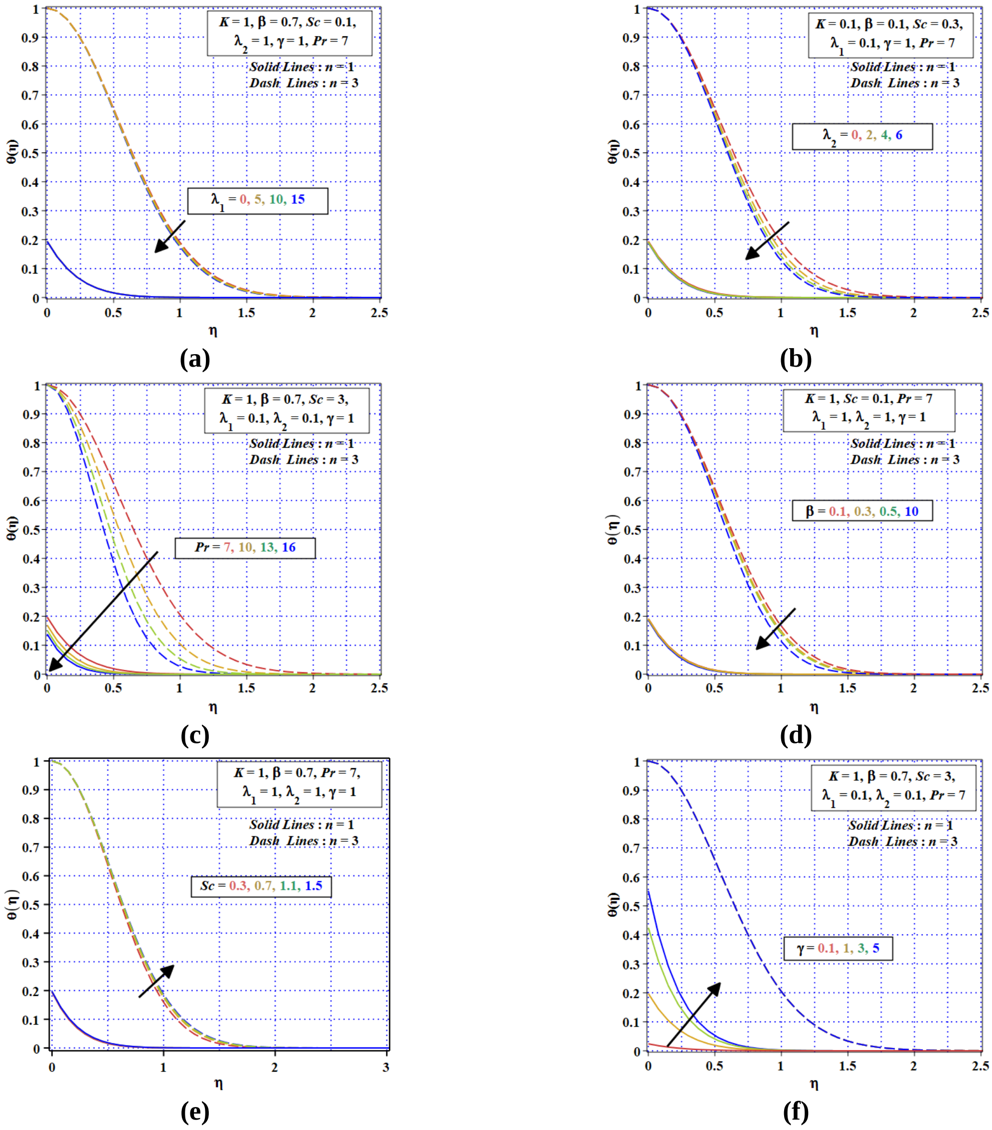

Figure 3. (a,b) Graphs of temperature profiles for various λ_1, λ_2 values; **(c,d)** Graphs of temperature profiles for various Pr, β values; **(e,f)** Graphs of temperature profiles for various Sc, γ values.

Figures 3a and 3b show that boundary layer thickness becomes thinner and thinner with the increase in λ_1 and λ_2 for the chemical reaction of order n=3. Further, when the chemical reaction is of order $n = 1$, there is a sharp reduction in temperature near the boundary followed by a decrease in boundary layer thickness with increasing values of λ_1 and λ_2. This is due to an increasing buoyancy effect, which accelerates fluid flow and enhances convective heat transfer near the boundary layer.

The temperature profile shown in Figure 3c exhibits a reduction as the Prandtl number increases, resulting in a decrease in the thickness of the boundary layer. This phenomenon is attributed to the Prandtl number representing the ratio of momentum diffusivity to thermal diffusivity. Thus, lower values of the Prandtl number facilitate the rapid diffusion of heat.

Figure 3d depicts a decrease in temperature profile with the increase in β when $n = 3$. A very slight variation is observed when $n = 1$.

Figure 3e depicts an increase in temperature profile with the increase in Sc. An increase in Sc lowers the flow velocity and causes an increase in the temperature profile, as Sc corresponds to the ratio of kinematic viscosity to the mass diffusivity.

Figure 3f portrays an increase in the temperature profile with the increase in γ for $n = 1$, and no variation exists in the temperature profile with the increase in γ for $n = 3$.

From Figures 3a, 3b, and 3e, it can be noted that temperature fields are less responsive in comparison with the velocity field to changes in parameters like λ_1, λ_2.

3.3. Effect on the concentration field.

Here, non-dimensional temperature $\phi(\eta)$ for different values of the parameters, namely λ_1, λ_2 β, K, Sc are plotted in Figure 4.

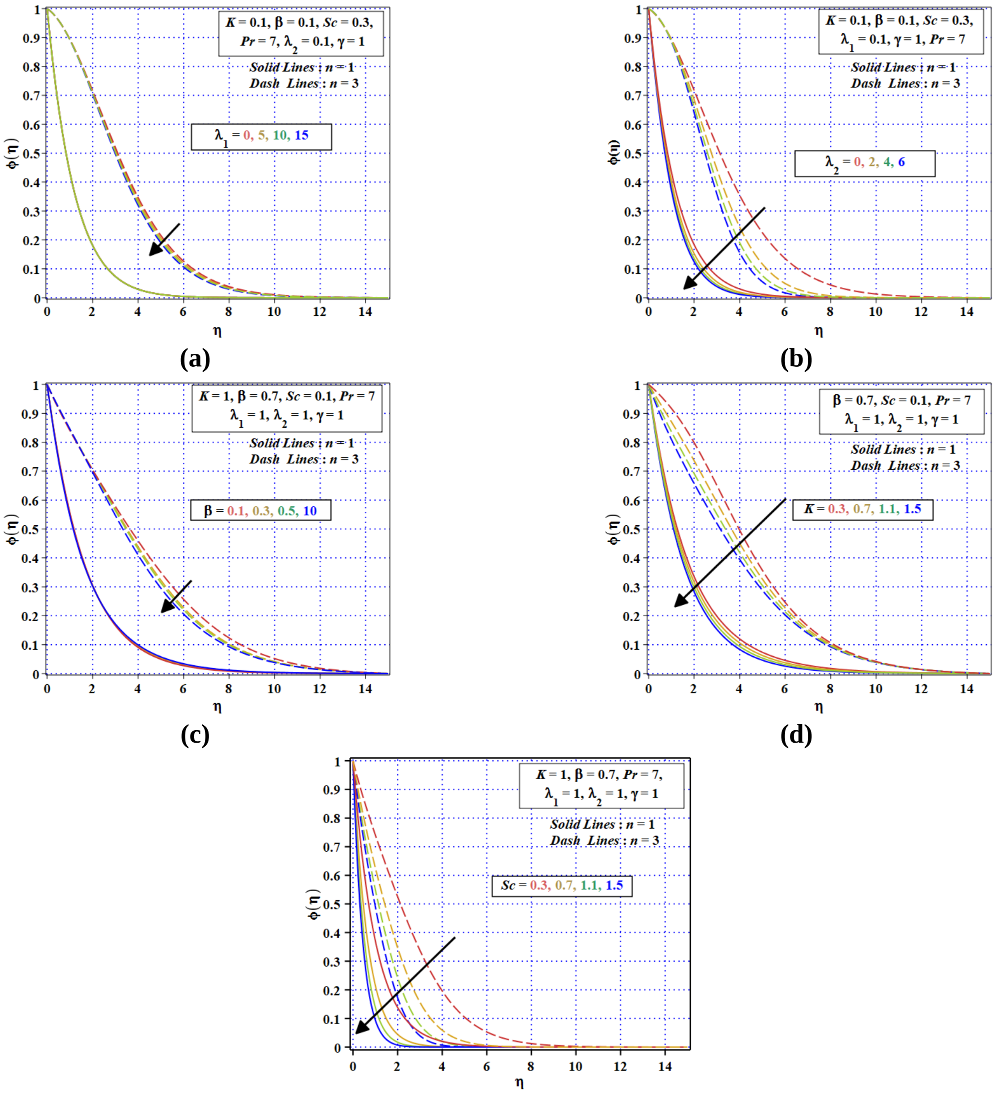

(e)

Figure 4. (a,b) Graphs of concentration profiles for various λ_1, λ_2 values; **(c,d)** Graphs of concentration profiles for various β, K values; **(e)** Graphs of concentration profiles for various Sc values.

Figure 4a depicts a decrease in concentration profile with an increase in λ_1.

It can be observed from Figure 4b that as λ_2 increases, the solutal boundary layer decreases. Further, it is noted that the concentration field is found to be less open to changes in λ_1 compared to λ_2.

From Figures 4c, 4d, and 4e, the thickness of the solutal boundary layer decreases in proportion to the increase in β, K, Sc parameters.

From the figures, it can be observed that the concentration field is more sensitive to changes in Sc than to any other parameter being investigated.

3.4. Skin friction coefficients.

Surface plots are plotted to analyze the effect of parameters $\beta, K, \lambda_1, \lambda_2, Sc$ on skin friction.

From the surface plot, Figure 5a, it can be observed that an increase in buoyancy parameters λ_1 and λ_2 results in a decrease in the skin friction factor. As a result, the boundary layer flow is accelerated because of the decrease in friction near the wall.

From the surface plot Figure 5b, it is clear that the $-f''(0)$ decreases for smaller values of K and Sc. As a result, the flow increases in the boundary layer.

From the surface plot Figure 5c, it is clear that the $-f''(0)$ decreases with the decrease in K and β.

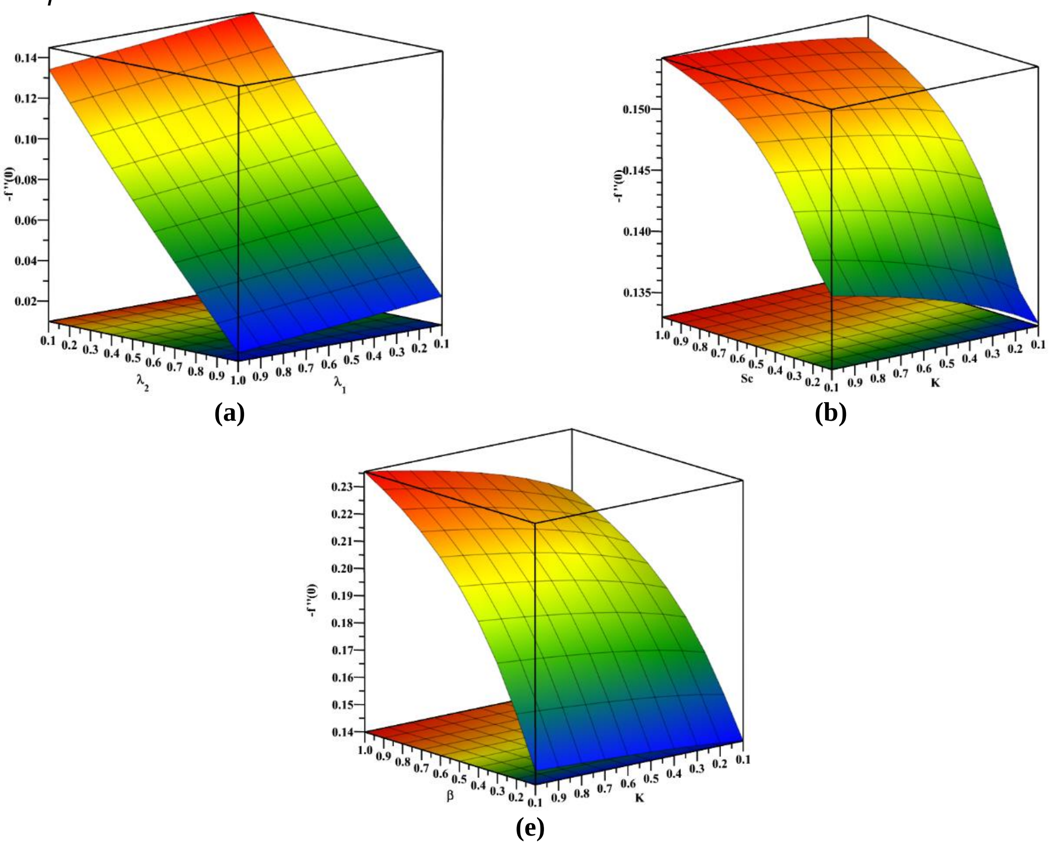

Figure 5. Surface plots of skin friction coefficient.

3.5. Nusselt number or heat flux.

Surface plots (Figure 6) are plotted to analyze the effect of parameters $\lambda_1, \lambda_2, Sc, K$ on heat flux. It is observed that heat transfer is more when $\lambda_1, \lambda_2, Sc, K$ are high.

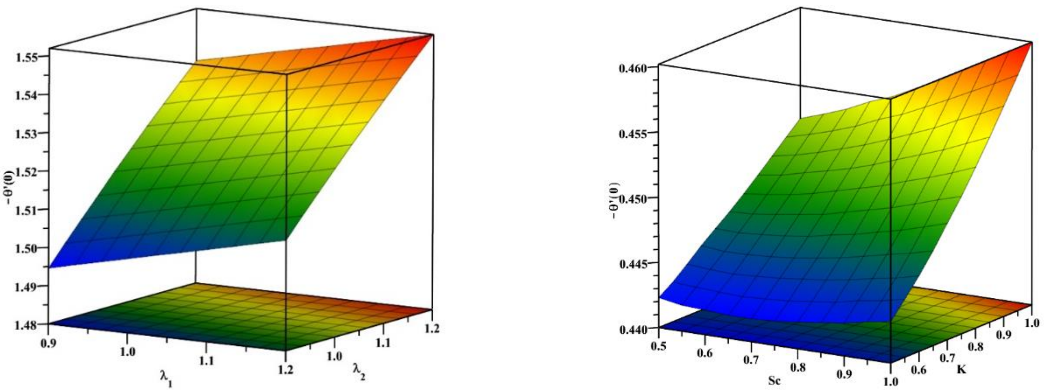

(a) **(b)**

Figure 6. Surface plots of Nusselt number.

3.6. Sherwood number.

Surface plots (Figure 7) are plotted to analyze the effect of parameters $\lambda_1, \lambda_2, Sc, K$ on Sherwood number. $-\phi'(0)$ increases with the increase in λ_1,λ_2, Sc and K.

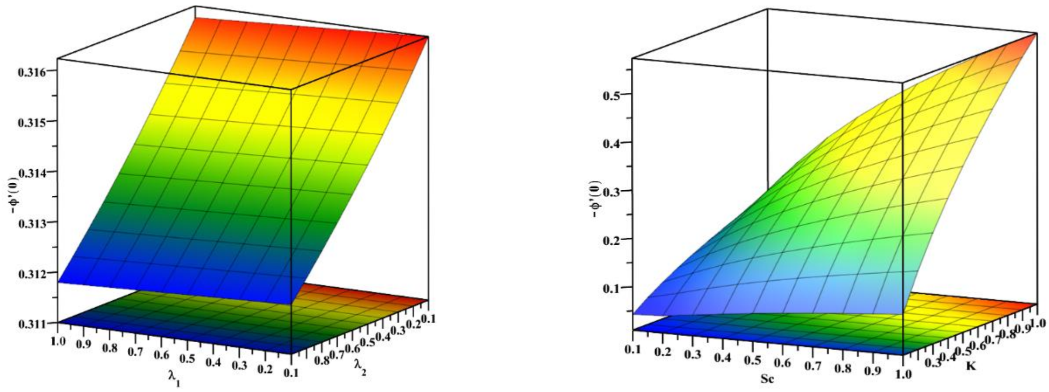

(a) **(b)**

Figure 7. Surface plots of Sherwood number.

In Table 1, multiple regression estimations for the local Nusselt number, local Sherwood number, and local skin friction are calculated using 100 sets of values of λ_1 and λ_2 which ranges from 0.1 to 1. Though linear fit is essential for all empirical problems, we fit the quadratic regression formula for better precision.

Table 1. Correlations for Nu_{est} $Sh_{est}$and Cf_{est} as a function of λ_1, λ_2.

Type	**Model**	**Adjusted R^2**
	Correlations for Nu_{est}	
Linear	$0.046342720\,\lambda_1 + 0.1450756\,\lambda_2 + 1.3230317$	0.9994
Quadratic	$1.2668 + 0.0543\lambda_1 + 0.2449\lambda_2 - 0.0066\lambda_1\lambda_2 - 0.0005{\lambda_1}^2 - 0.0442{\lambda_2}^2$	1.0000
	Correlations for Sh_{est}	
Linear	$-0.000228249\lambda_1 - 0.00468027\,\lambda_2 + 0.316588$	0.9974
Quadratic	$0.3168 - 0.0003\lambda_1 - 0.0057\lambda_2 + 0.0001\lambda_1\lambda_2 + 0.0009{\lambda_2}^2$	1.0000
	Correlations for Cf_{est}	
Linear	$-0.011523914\,\lambda_1 - 0.13376614\,\lambda_2 + 0.15770620$	0.9994
Quadratic	$0.1607 - 0.0121\lambda_1 - 0.1479\lambda_2 + 0.0009\lambda_1\lambda_2 + 0.0124{\lambda_2}^2$	1.0000

4. Conclusions

Fluids, with diverse types like ideal and real fluids, Newtonian and non-Newtonian fluids, exhibit unique behaviors, and certain ones, such as lubricating greases, polymers, and blood, defy classical Newton's law of viscosity. Researchers actively pursue the exploration of non-Newtonian fluids due to their wide-ranging applications and benefits across different fields. Hence, the present study focuses on the mixed convection flow of Casson fluid over a horizontally moving plate. The major outcomes of this investigation are summarized below:

The momentum boundary upsurges along with an overshooting in velocity profile with respect to the moving horizontal plate.

Momentum boundary layer thickness increases as the parameters λ_1, λ_2 increase. Conversely, the reverse nature is observed in the solutal and thermal boundary layers.

Momentum boundary layer thickness becomes thinner with the increase in β and K.

An increase in Pr and β reduces the solutal layer thickness, whereas the reverse nature is observed for the parameters Sc and γ.

Concentration profiles decrease with the increase in β and K.

An increase in $\beta, K,$ and Sc results in a 47.3%, 10%, and over 100% increase in the skin friction coefficient, respectively. Simultaneously, the acceleration of the boundary layer flow experiences a 15% increase for λ_1 and over 100% for λ_2.

Heat transfer is increased by 1% and 3% for the change of λ_1 and λ_2 respectively, while K contributes to a 5% enhancement in the same.

Linear regression model for the Nusselt number shows that an increase in $\lambda_1$and λ_2 upsurges the Nu_x whereas decreases the Cf_x.

The same is portrayed in the surface plots of the heat transfer factor and skin friction coefficient.

Funding

I hereby declare that there is no funding for the paper.

Acknowledgments

We are thankful to the institute for their support in facilitating our research.

Conflicts of Interest

The authors state that they do not have any conflicts of interest.

References

1. Uma, M.; Sushma, S.; Veena, B. N.; Srikantha, N. Study of solute transfer in presence of williamson fluid over exponentially stretching surfaces. *Iranian Journal of Chemistry and Chemical Engineering* **2023**, *42*, 2647-2654, https://doi.org/10.30492/IJCCE.2023.553525.5329.
2. Al-Kouz, W.;Owhaib, W. Numerical analysis of Casson nanofluid three-dimensional flow over a rotating frame exposed to a prescribed heat flux with viscous heating. *Scientific Reports* **2022,** *12*, 4256, https://doi.org/10.1038/s41598-022-08211-2.
3. Animasaun, I. L.; Adebile, E. A.; Fagbade A. I. Casson fluid flow with variable thermo-physical property along exponentially stretching sheet with suction and exponentially decaying internal heat generation using the homotopy analysis method. *Journal of the Nigerian Mathematical Society* **2016**, *35*, 1-17 https://doi.org/10.1016/j.jnnms.2015.02.001.
4. Bilal, S.; Asogwa, K. K.; Alotaibi, H.; Malik, M. Y.; and Khan, I. Analytical treatment of radiative Casson fluid over an isothermal inclined Riga surface with aspects of chemically reactive species. *Alexandria Engineering Journal* **2021**, *60*, 4243-4253, https://doi.org/10.1016/j.aej.2021.03.015.
5. Basavarajappa, M.; Lorenzini, G.; Srikantha, N.; Albakri, A.; Muhammad, T.; Heat Transfer of Nanomaterial over an Infinite Disk with Marangoni Convection: A Modified Fourier's Heat Flux Model for

Solar Thermal System Applications. *Applied Sciences* **2021**, *11*, 11609, https://doi.org/10.3390/app112411609.
6. Fan, J. R.; Shi, J. M.; Xu X. Z. Similarity solution of mixed convection over a horizontal moving plate. *Heat and Mass Transfer* **1997**, *32*, 199-206, https://doi.org/10.1007/s002310050112.
7. Khashi'ie, N. S.; Arifin, N. M.; Pop, I. Magnetohydrodynamics (MHD) boundary layer flow of hybrid nanofluid over a moving plate with Joule heating. *Alexandria Engineering Journal* **2022**, *61*, 1938-1945, https://doi.org/10.1016/j.aej.2021.07.032.
8. Mohd Rohni, A.; Ahmad, S.; Pop, I.; Boundary layer flow over a moving surface in a nanofluid beneath a uniform free stream. *International Journal of Numerical Methods for Heat & Fluid Flow* **2011**, *21*, 28-846, https://doi.org/10.1108/09615531111162819.
9. Pramanik, S. Casson fluid flow and heat transfer past an exponentially porous stretching surface in presence of thermal radiation. *Ain Shams Engineering Journal* **2014**, *5*, 205-212, https://doi.org/10.1016/j.asej.2013.05.003.
10. Khan W. A.; Uddin M.; Ismail A. I. Similarity solutions of MHD mixed convection flow with variable reactive index, magnetic field, and velocity slip near a moving horizontal plate: a group theory approach. *Mathematical Problems in Engineering* **2012**, 183029, https://doi.org/10.1155/2012/183029.
11. Sushma, S.; Neeraja, G.; Dinesh, P. A.; Uma, M.; Samuel, N. Analysis of Wavering MHD and Chemical Reaction on Casson Fluid Flow over a Stretching Sheet. *Mathematical Models and Computer Simulations* **2022**, *14*, 349-356, https://doi.org/10.1134/S2070048222020119.
12. Shaw, S.; Mahanta, G.; and Sibanda, P. Non-linear thermal convection in a Casson fluid flow over a horizontal plate with convective boundary condition. *Alexandria Engineering Journal* **2016**, *55*, 1295-1304, https://doi.org/10.1016/j.aej.2016.04.020.
13. Sulochana, C.; Poornima, M. Unsteady MHD Casson fluid flow through vertical plate in the presence of Hall current. *SN Applied Sciences* **2019**, *1*, 1-14, https://doi.org/10.1007/s42452-019-1656-0.
14. Khan, K. A.; Jamil, F.; Ali, J.; Khan, I.; Ahmed, N.; Andualem, M.; Rafiq, M. Analytical simulation of heat and mass transmission in casson fluid flow across a stretching surface. *Mathematical Problems in Engineering* **2022**, 1-11, https://doi.org/10.1155/2022/5576194.
15. Thamaraikannan, N.; Karthikeyan, S.; Chaudhary, D. K. Significance of MHD radiative non-Newtonian nanofluid flow towards a porous channel: a framework of the Casson Fluid Model. *Journal of Mathematics* **2021**, 9912239, https://doi.org/10.1155/2021/9912239.
16. Kumar, C. K.; Srinivas, S.; Reddy, A. S. MHD pulsating flow of Casson nanofluid in a vertical porous space with thermal radiation and Joule heating. *Journal of Mechanics* **2020**, *36*, 535-549, https://doi.org/10.1017/jmech.2020.5.
17. Srinivas, S.; Kumar, C. K.; Reddy, A. S. Pulsating flow of Casson fluid in a porous channel with thermal radiation, chemical reaction and applied magnetic field. *Nonlinear Analysis: Modelling and Control* **2018**, *23*, 213-233, https://doi.org/10.15388/NA.2018.2.5.
18. Shankar, S.; Ramakrishna, S.R.; Gullapalli, N.; Samuel, N. Triple diffusive MHD Casson fluid flow over a vertical wall with convective boundary conditions. *Biointerface Research in Applied Chemistry* **2021,** *11*, 13765-13778, https://doi.org/10.33263/BRIAC116.1376513778.
19. Alwawi, F. A.; Alkasasbeh, H. T.; Rashad, A. M.; Idris, R.; MHD natural convection of Sodium Alginate Casson nanofluid over a solid sphere. *Results in physics* **2020**, *16*,102818, https://doi.org/10.1016/j.rinp.2019.102818.
20. Alwawi, F.A.; Alkasasbeh, H.T.; Rashad, A.M.; Idris, R. A. Numerical approach for the heat transfer flow of carboxymethyl cellulose-water based Casson nanofluid from a solid sphere generated by mixed convection under the influence of Lorentz force. *Mathematics* **2020**, *8*, 1094, https://doi.org/10.3390/math8071094.
21. Hamarsheh, A.S.; Alwawi, F.A.; Alkasasbeh, H. T.; Rashad, A. M.; Idris, R. Heat transfer improvement in MHD natural convection flow of graphite oxide/carbon nanotubes-methanol based casson nanofluids past a horizontal circular cylinder. *Processes* **2020**, *8*, 1444, https://doi.org/10.3390/pr8111444.
22. El-Zahar, E. R.; Mahdy, A.E.N.; Rashad, A.M.; Saad, W.; Seddek, L.F. Unsteady MHD mixed convection flow of Non-Newtonian Casson hybrid nanofluid in the stagnation zone of sphere spinning impulsively. *Fluids* **2021**, *6*, 197, https://doi.org/10.3390/fluids6060197.
23. El-Zahar, E. R.; Rashad, A.M.; Al-Juaydi, H.S.; Studying massive suction impact on magneto-flow of a hybridized Casson nanofluid on a porous continuous moving or fixed surface. *Symmetry* **2022**, *14*, 627, https://doi.org/10.3390/sym14030627.

24. Atashafrooz, M. The effects of buoyancy force on mixed convection heat transfer of MHD nanofluid flow and entropy generation in an inclined duct with separation considering Brownian motion effects. *Journal of Thermal Analysis and CalorimetryI* **2019**, *138*, 3109-3126, https://doi.org/10.1007/s10973-019-08363-w.
25. Lone, S.A.; Anwar, S.; Saeed, A.; Bognár, G. A stratified flow of a non-Newtonian Casson fluid comprising microorganisms on a stretching sheet with activation energy. *Scientific Reports*. **2023**, *13*, 11240, https://doi.org/10.1038/s41598-023-38260-0.
26. Priyanka, P.; Abdelmohsen, S.A.; Tawade, J.V.; Ashraf, A.M.; Kumar, R.; Biradar, M.M. Multiple slip effects of MHD boundary-layer motion of a Casson nanoliquid over a penetrable linearly stretching sheet embedded in non-Darcian porous medium. *International Journal of Modern Physics B* **2023**, *37*, 2350022, https://doi.org/10.1142/S0217979223500224.
27. Vishalakshi, A.B.; Mahabaleshwar, U.S.; Ahmadi, M.H.; Sharifpur, M. An MHD Casson fluid flow past a porous stretching sheet with threshold Non-Fourier heat flux model. *Alexandria Engineering Journal* **2023**, *69*, 727-37, https://doi.org/10.1016/j.aej.2023.01.037.
28. Al-Sharifi, H.A.; Kasim, A.R.; Hussanan, A. Numerical investigation of Casson micropolar fluid over a stretching sheet with convective boundary condition. In *AIP Conference Proceedings* **2023**, *13*, https://doi.org/10.1063/5.0114702.
29. Seethamahalakshmi, V.; Rekapalli, L.; Rao, T.S.; Santoshi, P.N.; Reddy, G. V.; Oke, A.S. MHD slip flow of upper-convected Casson and Maxwell nanofluid over a porous stretched sheet: impacts of heat and mass transfer. *CFD Letters* **2024**, *16*, 96-111, https://doi.org/10.37934/cfdl.16.3.96111.
30. Reddy, B. N.; Maddileti, P.; Chesneau, C. Stagnation point on MHD boundary layer flow of heat and mass transfer over a non-linear stretching sheet with effect of Casson nanofluid. *International* Journal of Modelling and Simulation **2023**, *29*, 1-3, https://doi.org/10.1080/02286203.2023.2286420.
31. Majeed, A.; Rifaqat, S.; Zeeshan, A.; Alhodaly, M.S.; Majeed Noori, F. Impact of velocity slip and radiative magnetized Casson nanofluid with chemical reaction towards a nonlinear stretching sheet: Three-stage Lobatto collocation scheme. *International Journal of Modern Physics B.* **2023**, *7*, 2350088, https://doi.org/10.1142/S0217979223500881.
32. Ali, L.; Kumar, P.; Poonia, H.; Areekara, S.; Apsari, R. The significant role of Darcy–Forchheimer and thermal radiation on Casson fluid flow subject to stretching surface: A case study of dusty fluid. *Modern Physics Letters B* **2024**, *38*, 2350215, https://doi.org/10.1142/S0217984923502159.
33. Goud, B.S.; Reddy, Y.D.; Asogwa, K.K. Chemical reaction, Soret and Dufour impacts on magnetohydrodynamic heat transfer Casson fluid over an exponentially permeable stretching surface with slip effects. *International Journal of Modern Physics B* **2023**, *37*, 2350124, https://doi.org/10.1142/S0217979223501242.
34. Lone, S.A.; Shamshuddin, M.D.; Shahab, S.; Iftikhar, S.; Saeed, A.; Galal, A.M. Computational analysis of MHD driven bioconvective flow of hybrid Casson nanofluid past a permeable exponential stretching sheet with thermophoresis and Brownian motion effects. *Journal of Magnetism and Magnetic Materials* **2023**, *580*, 170959, https://doi.org/10.1016/j.jmmm.2023.170959.
35. Biswal, M. M.; Swain, K.; Dash, G.C.; Mishra, S. Study of chemically reactive and thermally radiative Casson nanofluid flow past a stretching sheet with a heat source. *Heat Transfer* **2023**, *52*, 333-53, https://doi.org/10.1002/htj.22697.